Ethanol based fuel cell on paper support

Subrata Chandra[a,1], Sweta Lal[b,1], Vinod M. Janardhanan[b,*], Kirti Chandra Sahu[b,*], Melepurath Deepa[a,*]

[a]*Department of Chemistry, Indian Institute of Technology Hyderabad, Sangareddy 502 285, Telangana, India*
[b]*Department of Chemical Engineering, Indian Institute of Technology Hyderabad, Sangareddy 502 285, Telangana, India*

Abstract

Easily disposable low cost fuel cells as power sources are environmentally benign alternates to batteries for powering micro-analytical systems. In this regard, for the first time, an ethanol-dichromate fuel-oxidant microfluidic fuel cell is implemented on a paper scaffold. In this cell, a proton conducting poly (4-styrenesulfonate) based gel electrolyte enables proton transport from the anode to the cathode. Hydrothermally synthesized molybdenum oxide nanorods catalyze dichromate reduction and ethanol oxidation at the respective electrodes. A peak power density of 6.32 $mWcm^{-2}$ is achieved with the catalyst. However, the cell without catalyst delivers a maximum power density of only 2.74 $mWcm^{-2}$. The compositions of the catholyte and anolyte streams and molybdenum oxide loadings are optimized. A stack of two cells connected in series illuminates a 3 mm red light emitting diode for over 40 minutes. This real time demonstration showcases the potential of this cell as an alternative to batteries for powering micro-analytical devices.

Keywords: Ethanol; Paper support; Fuel cells; Carbon; MoO3

1. Introduction

In recent times, energy conversion devices which rely on the self transporting property of paper for metering reactants have received significant interest from researchers worldwide as these de-

*Corresponding author
Email addresses: vj@iith.ac.in (Vinod M. Janardhanan), ksahu@iith.ac.in (Kirti Chandra Sahu), mdeepa@iith.ac.in (Melepurath Deepa)
[1]Equal contribution

vices can be easily integrated into micro total analysis systems (μ-TAS) and lateral flow diagnostic devices such as glucometers, dengue test kits, pregnancy detection kits, paper based centrifuge for blood processing and paper machine for molecular diagnostics [1–3]. Moreover, paper is ubiquitious, bio-degradable and can be cut into any shape. These devices can be made from low cost, easily available and easily disposable components, and do not require pumps or moving parts. A variety of cell architectures with the sole objective of miniaturization of paper-based microfluidic devices have been proposed [4, 5]. Use of these devices in point of care diagnostic devices can revolutionize rural health care. Paper based fuel cells, which rely on the parallel laminar flow of anolyte and catholyte utilizing different fuels such as methanol, hydrogen peroxide and formic acid have been demonstrated recently [6, 7]. In the case of parallel flow membraneless fuel cells, an electrolyte phase is required for the transport of ions from one electrode to the other. Therefore, the fuel and oxidant needs to be mixed with electrolytes to form the anolyte and catholyte. Although the cell performances reported in such systems are fairly good, the fuel/oxidant cross-over continues to limit the cell performance in membraneless configurations. Paper-based fuel cells with poly(acryl amide) based proton conducting gel as a separating membrane to limit the anolyte/catholyte cross over, with relatively stable and regenerative cell performances, have also been reported [8]. These systems can maintain the open circuit voltage (OCV) of the cell without appreciable drop over time as compared to the membraneless configurations.

The fuel-oxidant redox couple plays a key role in deciding the electrochemical performance of a fuel cell. Ideally, the redox couple chosen should deliver a high standard potential and the cell reactions should not lead to the formation of hazardous by-products. Besides these aspects, the electrolyte used for forming the anolyte and catholyte should have appreciable ionic conductivity to facilitate easy transport of ions within the system. While many fuel-oxidant pairs using different acidic and alkaline electrolytes have been reported in the literature, the ethanol-dichromate fuel-oxidant combination has not been reported so far to the best of our knowledge. Ethanol is low cost, enviroment friendly, easily available, easy to store and handle, and has a high energy

density (8.0 kWh kg^{-1}) [9, 10]. On the other hand, potassium dichromate ($K_2Cr_2O_7$) is cheap, non-toxic and a strong oxidizing agent. Due to the slow electrochemical oxidation kinetics of ethanol, various metal-based catalysts and binary metal catalysts (e.g. Pt-Ru, Pt-Sn), trimetallic catalyst (e.g. Pt-Ru-Ni, Pt-Sn-Ni) and carbon supported metal catalysts (e.g. Pt/C, Pd/ MWCNTs, PdAg/MWCNTs (multiwalled carbon nanotubes)) have been used as anode catalysts to enhance the kinetics.

These electrocatalysts have shown promising performances in direct ethanol based fuel cells (DEFC) and microfluidic fuel cells [9, 11, 12]. However, due to high cost and limited availability, these noble metal based catalysts cannot be used for developing low cost paper based fuel cells. Molybdenum oxide (MoO_3) is an inexpensive alternative to the above mentioned catalysts. MoO_3 has a good ethanol sensing property [13], and by preparing the same in nanostructured form, the catalytic surface area can be enhanced, which can lead to high oxidation currents. While a composite of MoO_3 with poly(pyrrole) has been used as a support for Pt-Pd nanoparticles for ethanol electro-oxidation in DEFC [14], MoO_3 as a stand-alone catalyst in paper based ethanol fuel cell has not been reported so far.

In the present study, solution phase ethanol-dichromate fuel cell is developed using filter paper as support at the room temperature. A proton conducting poly (4- styrenesulfonate) (PSS) based gel is used to maximize the cell performance. Hydrothermally synthesized MoO_3 nanorods (NRs) loaded onto carbon cloth/stainless steel (SS/carbon cloth) assembly are employed as electrodes. Elaborate studies are carried out by using different fuel/oxidant compositions and catalyst loadings. It is also demonstrated that a stack of two cells connected in series and packed into acrylic boxes can illuminate an LED. This illustrates the potential of the present cell as an alternative to batteries to power micro-analytical electronic devices.

The rest of the paper is organised as follows. The experimental set-up and procedure are presented in Section 2. Here, the cell assembly, preparation of membrane and electrodes, and instrumentation are discussed. The practical demonstration of the cells to light an LED is also

provided at the end of this section. The results are discussed in Section 3. The concluding remarks are provided in Section 4.

2. Experimental

2.1. Cell assembly

The cell was assembled by placing two L-shaped paper strips 0.2 cm apart, and the sodium poly(4-styrenesulfonate) (Na-PSS) gel was placed in between the strips as shown in the inset of Fig. 1(a).

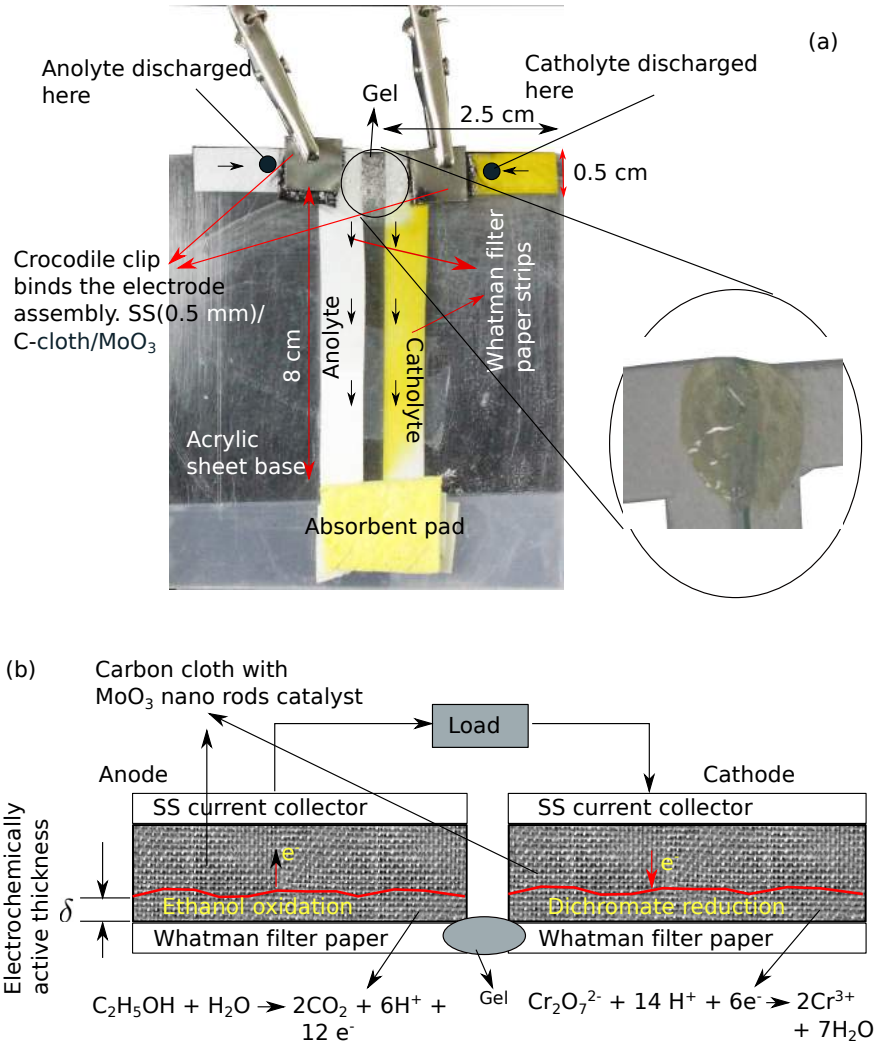

Figure 1: (a) Photograph of the cell assembly and (b) Schematic of the cross sectional views of the anode and cathode.

The thickness of the gel membrane is 0.5 mm. The gel acts as a proton exchange membrane for the transport of ions. The Na-PSS/PVA/H^+ gel was placed using a spatula in the space between the two L-joints of the two paper strips. Figure 1(b) shows the schematic of the cross-sectional views of the electrodes with descriptions of the electrochemically active thicknesses over which the reactions take place. It is not possible to determine the actual thickness of the electrochemically active layer, which is denoted by δ in Fig. 1(b). The electrons, which are released in the electrochemically active layer at the anode, are conducted by the carbon cloth and collected by the SS current collector and transported to the cathode, where dichromate ions undergo reduction. Figure 1(b) also shows the electron transfer path. Aqueous solutions containing varying concentrations of C_2H_5OH (2 M, 3 M, 4 M, 5 M, and 6 M) along with 4 M H_2SO_4 (electrolyte) are used as the anolytes. Aqueous solutions of 0.3 M $K_2Cr_2O_7$ (oxidant) along with 4 M H_2SO_4 are used as the catholytes and 0.2 ml each of anolyte and catholyte are used. The short arm (0.5 cm $\times$ 2.5 cm) of each L-shaped paper strip serves as the inlet for the anolyte/catholyte, and the longer arm (0.5 cm $\times$ 8 cm) serves as the outlet for the products and unused reactants, as shown in Fig. 1(a). Carbon cloth of size 0.5 cm $\times$ 0.7 cm is placed on the inlet arm of the L-shaped paper strip, which serve as the electrodes. Since the electrodes are in contact with the electrolyte phase present in the fuel and oxidant, the geometric area (0.35 cm^2) of the electrodes is used to calculate the current density. Steel plates of dimensions equal to the electrode are used as the current collectors. The by-products and unreacted species flow by the capillary action towards the outlets, i.e. the longer arms. The objective of keeping the outlet strip long is to avoid the back flow of the by-products to the electrodes and the gel, which can otherwise interfere with the cell reactions by diluting anolyte and catholyte. Since ethanol is volatile, the length of the inlet arm is kept short so that once the anolyte/catholyte containing the fuel/oxidant are discharged near the electrodes, they are immediately utilized. An absorbent pad is placed at the bottom of the cell to absorb the products and the unused reactants. The absorbent pad used in the cell is basically a spongy material (similar to kitchen wipe) having 3 mm thickness. The paper used is a Whatman filter paper (ashless 42) of

thickness 0.13 mm. The anolyte and catholyte are discharged near electrodes using a pipette. The whole assembly is placed on an acrylic sheet.

2.2. Preparation of Na-PSS/PVA/H^+ gel/membrane

A solution was prepared by dissolving 2 g of Na-PSS/H^+ in 10 mL of deionized water. The resulting solution was stirred at 500 rpm and heated at a temperature of 75 ^oC for 10 minutes. Once the solution was completely homogeneous, 0.8 g of poly(vinyl acetate) (PVA) was added and stirring was continued for another 45 minutes to make the solution sufficiently viscous. PVA acts as a gelatinizing agent and imparts mechanical strength to the gel. After the stirring was complete, the viscous gel was cooled at room temperature. The final yellow coloured substance was referred to as Na-PSS/PVA/H^+ gel or membrane. The proton exchange in Na-PSS/PVA/H^+ gel occurs at the sulfonate moiety ($-SO_3Na$ to $-SO_3H$). The pH of the gel was 5-6 as measured by a pH paper.

2.3. Synthesis of MoO_3 NRs and electrode preparation

MoO_3 NRs were synthesized hydrothermally according to the procedure described elsewhere [15]. 1 g of ammonium heptamolybdate ($(NH_4)_6Mo_7O_{24}\cdot 4H_2O$) was dissolved in 40 ml solution containing 65% HNO_3 and deionized water (HNO_3:H_2O, v/v 1:5). After complete dissolution of $(NH_4)_6Mo_7O_{24}\cdot 4H_2O$, the above solution was transferred to a 50 ml teflon cup and placed in a stainless steel autoclave. This was then placed in an electric oven and heated at a temperature of 180 ^oC for 12 hours. The solution was then cooled to room temperature and centrifuged to extract the MoO_3 NRs. These were then washed with copious amounts of ultra-pure water and the black precipitate was dried overnight in a hot-air-oven at 60 ^oC. Carbon cloth of size 0.5 cm $\times$ 0.7 cm was used as electrodes. 10 mg of the MoO_3 powder was dissolved in 10 ml of toluene and drop cast onto the carbon cloth electrodes by a pipette. Electrodes with variable catalyst loadings were prepared to study the effect of catalyst loading.

2.4. Instrumentation

The electrochemical measurements of the cells, i.e., chronoamperometry (*I vs t*), chronopotentiometry (*V vs t*), electrochemical impedance spectroscopy (EIS) and cyclic voltammetry (CV) were done on an Autolab PGSTAT 302N with a frequency response analyzer and integrated NOVA 1.11 software. The structure and morphology of the prepared MoO_3 NRs catalyst were studied using a Zeiss field emission scanning electron microscope (FE-SEM) by obtaining the micrographs for the catalysts. Transmission electron microscope (JEOL JEM2100) with a resolution of 2.3Å was used for characterizing the catalyst. The powder sample (MoO_3) was dispersed in isopropanol, and a thin layer of the solution was placed onto carbon coated copper grids. The samples were then analyzed after isopropanol was evaporated from the deposited layers.

3. Results and discussion

3.1. Structural features of MoO_3 NRs

Prior to studying the fuel cell performances, the structure and morphology of the prepared MoO_3 NRs are studied by FE-SEM and TEM. The FE-SEM images of MoO_3 NRs are shown in Fig. 2(a) and (b). Both the images are obtained at low magnification and they show bundles of misaligned and monodispere nanorods. The corressponding TEM images are shown in Fig. 2(c)-(e). At low resolution, the nanorods overlap with each other, but at high resolution (Fig. 2(d)) distinct formation of nanorods with uniform width along the length are observed. The surfaces appear to be smooth. The diameter and length of the nanorods vary from 50 nm to 125 nm and from 800 nm to 2 μm, respectively. The aspect ratio (L/D) for these nanorods ranges from 6 to 22. The selected area electron diffraction (SAED) pattern, for MoO_3 NRs is shown in Fig. 2(f). The bright single spots are due to the beam diffraction by a single crystal, which confirms the crystallinity of the synthesized MoO_3 NRs. The spots are indexed to the (011), (111) and (101) planes of the orthorhombic crystal structure of MoO_3. Similar SAED patterns for MoO_3 NRs have been reported by other researchers as well [15, 16].

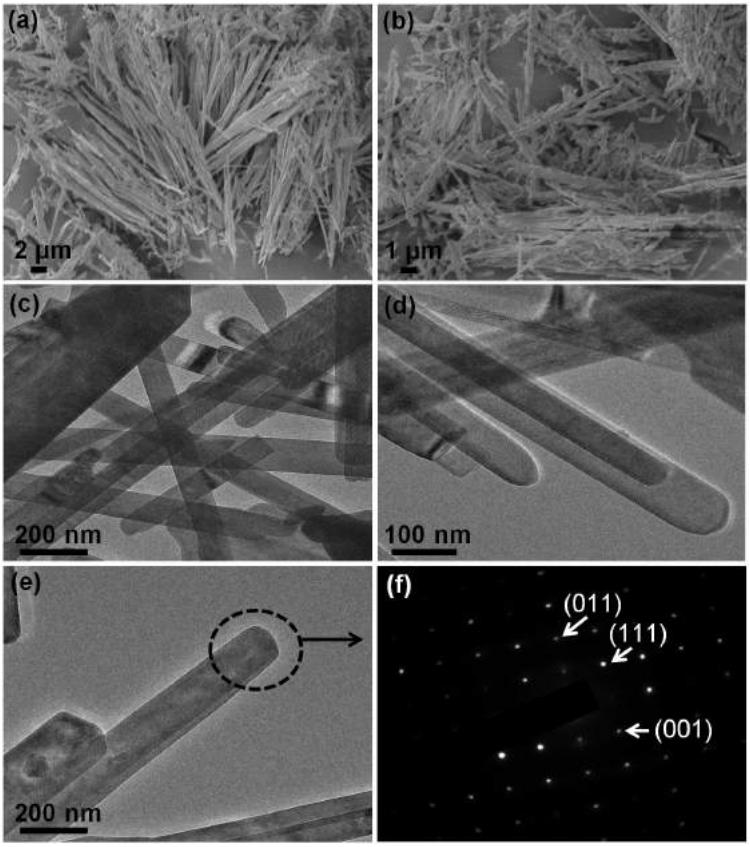

Figure 2: (a) and (b) FE-SEM images of MoO_3 NRs. (c)-(e) TEM images MoO_3 NRs and (f) the corresponding SAED pattern of a MoO_3 NR.

3.2. Electrochemical performance and gel characterization

The cell relies on the oxidation of ethanol at the anode for the production of electrons and protons. The electrons reach the cathode via the external circuit, and simultaneously the protons migrate to the cathode though the Na-PSS/PVA/H^+ gel electrolyte. Dichromate ions (oxidant) undergo reduction at the cathode by accepting the electrons from the anode. These reactions can ideally occur at any location where the carbon cloth (with or without MoO_3 NRs) comes in contact with the anolyte/catholyte. The oxidation of ethanol follows complex pathways leading to the formation of acetaldehyde and acetic acid as by-products. The formation of CO is also reported previously [17]. The reduction of dichromate at the cathode is given by

$$Cr_2O_7^{2-} + 14H^+ + 6e^- \rightleftharpoons 2Cr^{3+} + 7H_2O, \quad (1)$$

It can be seen in the reaction that, Cr^{6+} in $Cr_2O_7^{2-}$ reduces to Cr^{3+}. Being a transition metal ion, Cr^{3+} can exist as an aquo-complex, $[Cr(H_2O)_6]^{3+}$ in solution. The oxidation reaction at the anode is given by

$$C_2H_5OH + H_2O \rightarrow 2CO_2 + 12H^+ + 12e^-. \quad (2)$$

The overall cell reaction is given by

$$16H^+ + 2Cr_2O_7^{2-} + C_2H_5OH \rightarrow 4Cr^{3+} + 11H_2O + 2CO_2. \quad (3)$$

It is generally accepted that multiple electron transfer reactions are rare in reality and therefore, the actual mechanism of oxidation of ethanol can be expected to be multi-step, eventually culminating with the formation of either CO or CO_2. At the cathode, dichromate reduction is accompanied by the conversion of Cr (VI) to Cr (III) species. Cyclic voltammeter (CV) plots were recorded to study ethanol oxidation (4 M ethanol in 4 M H_2SO_4) in an aqueous acidic medium at a scan rate of 20 mV s^{-1} with Ag/AgCl/KCl as a reference electrode and a Pt rod as a counter electrode. CV plots of carbon cloth loaded with MoO_3 NRs and blank carbon cloth (as working electrodes) are shown in Fig. 3. The voltage is swept back and forth from -0.5 to 2.0 V (versus Ag/Ag^+) at a scan rate of 20 mV s^{-1}.

To understand the influence of MoO_3 NRs in the electro-oxidation of ethanol, experiments are initially performed without MoO_3 on the carbon cloth. The nonappearance of peaks in the forward and reverse sweeps indicates the absence of diffusion layer formation or depletion effects. The presence of two broad shoulders clearly indicates that the oxidation of ethanol is governed by multi-step charge transfer reactions involving different species that are electrochemically active. The first shoulder is observed at approximately 0.48 V. The two different shoulders in the

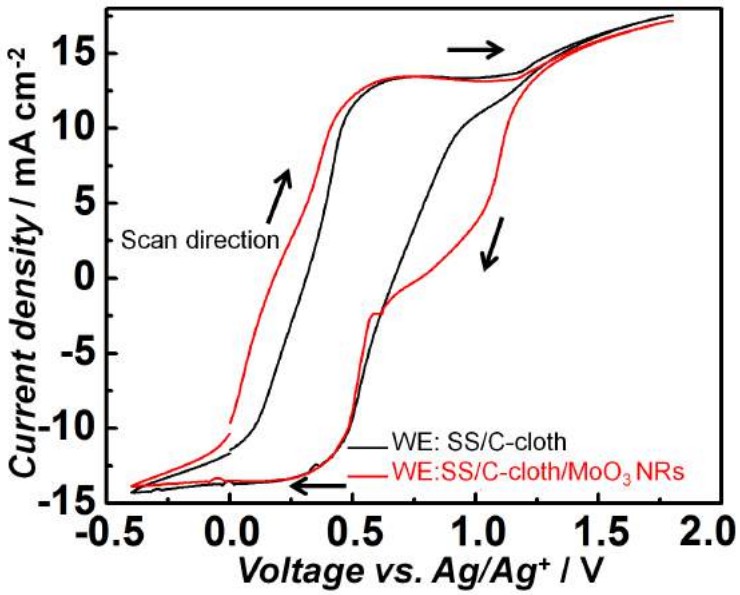

Figure 3: Cyclic voltammograms for ethanol-oxidation with MoO_3 NRs loaded carbon cloth and blank carbon cloth as working electrodes.

forward sweep correspond to two different rate limiting charge transfer reactions. On reversing the potential, the curve traces back the forward sweep until the first shoulder, indicating that there is an abundance of surface adsorbed species responsible for electron transfer at the electrode. i.e., on reversing the potential, the current is still anodic, until the first shoulder. The reduction current starts flowing on reducing the potential further. The behavior is same with and without MoO_3 NRs, except that the presence of MoO_3 NRs increases the area enclosed in the voltammogram, implying that MoO_3 NRs show good electrocatalytic activity for ethanol oxidation. Since the Na-PSS/PVA/H^+ gel electrolyte is used as membrane to facilitate the transport of ions (primarily protons or H^+) between the electrodes, the conductivity of gel is measured by performing EIS. Na-PSS/PVA/H^+ is a polyelectrolyte and SO_3^- Na^+ groups present along the backbone of the polymer chain, serve as the active sites for the transport of protons. The SO_3^- groups are attached to the backbone of the polymer poly(styrene) and are immobile. The Na^+ ions are replaced by H^+ ions which are released from the dissociation of H_2SO_4 in the gel. The charge transfer mechanism is believed to be the same as the one that prevails in a Nafion membrane.

The conductivity of the gel is measured by placing the gel electrolyte between two steel plates under an ac-amplitude of 10 mV without any dc bias over a frequency range of 1 MHz-1 kHz. The resulting Nyquist plot (Fig. S1(a) of the supplementary material) shows an inclined line. The high frequency intercept on the abscissa corresponds to the resistance (R) offered by the gel for H^+ movement. The conductivity of the gel (σ) is calculated using $\sigma = (1/\mathrm{R}) \times (l/a)$, where l (cm) is the thickness of the gel layer and a (cm^2) is the area of the SS plates in contact with the gel. At room temperature this resulted in 0.063 S cm^{-1}. The conductivity of the gel as a function of temperature is shown in Fig. S1(b). The conductivity of the gel increases with temperature due to enhanced mobility of H^+ ions at high temperatures. At room temperature, the gel is transparent, homogeneous and yellow in color. At temperatures above 55 ^{o}C, it becomes opaque. The Na-PSS/PVA/H^+ gel can therefore be used upto 50 ^{o}C. In the present study, all the cells are assembled and studied at room temperature. For the electrochemical charge transfer reaction to occur, a three phase interface between ion conducting phase, electron conducting phase and the fuel/oxidant is required. In the present study, ion transport occurs due to the presence of H_2SO_4, which is added to the fuel and the oxidant in order to form the anolyte and the catholyte, respectively. Carbon cloth is used as the electron conducting phase. Thus a three phase interface is formed where ever the carbon cloth threads come in contact with the anolyte and catholyte. The three phase interfaces are located within the electrochemically active region shown in Fig. 1(b). Due to the presence of H_2SO_4 throughout the system, a physical contact of the gel membrane with the electrodes is strictly not required for the progress of the charge transfer reaction. Thus in this work, the two paper strips are completely disconnected when the gel is not placed between them. The gel acts as a bridge for the transport of ions from the anode to the cathode, and without the presence of gel between the electrodes, the cell will not be able to generate power. Cells are assembled on paper supports with SS/carbon-cloth as the electrodes and a Na-PSS/PVA/H^+ gel. The electrochemical performance of the cell is studied by varying the fuel or ethanol concentration from 2 to 6 M, in 4 M H_2SO_4, while keeping the concentration of catholyte constant (0.3 M $K_2Cr_2O_7$ + 4 M H_2SO_4).

Carbon cloth without any catalyst loading is used as the electrode. A new cell is prepared and used every time the fuel concentration is changed.

The dc-polarization curves for different fuel concentrations are shown in Fig. 4(a) and (b).

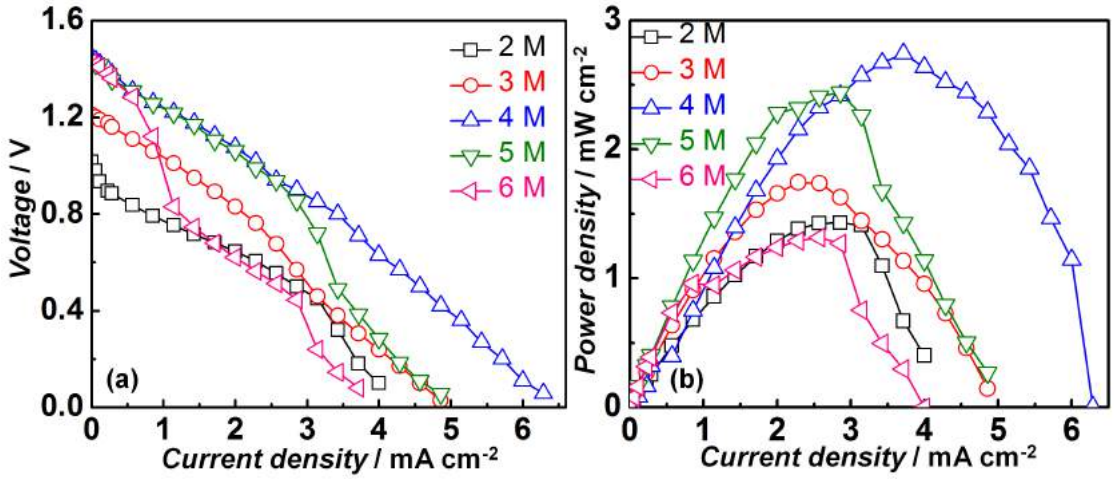

Figure 4: Cell performance at various ethanol concentrations in 4 M H_2SO_4. The catholyte is an aqueous solution of 0.3 M $K_2Cr_2O_7$ + 4 M H_2SO_4. SS/carbon cloth are used as the electrodes.

The cell delivers low open circuit voltage (OCV) at low concentrations of 2 and 3 M, and higher OCVs at 4 M, 5 M and 6 M ethanol, which is due to the dependence of reversible voltage on concentration according to Nernst equation. The standard potential term in the Nernst equation is independent of concentration and the concentration dependent term is $-(RT/nF)\ln(\prod a_p^{\nu_i} / \prod a_r^{\nu_i})$. The absolute value of this term increases with the increase in the activity of the reactants for a given activity of the products. The overall cell performance is poor at low and high concentrations of ethanol (Fig. 4(b)). At low concentrations, the poor cell performance is due to the low Faradaic reaction rates because of the concentration dependency of exchange current density. It is well known that the ethanol oxidation kinetics is slow, and hence higher concentrations are required for higher reaction rates and better cell performance. However, at higher concentrations of ethanol, cross-over to the cathode through the Na-PSS/PVA/H^+ gel is high, which again leads to a poor cell performance. In order to verify this, a control experiment or a paper wetness test is performed.

The Na-PSS/PVA/H^+ gel is placed between two paper strips and ethanol is discharged near the anode. Ethanol starts to diffuse across the gel membrane to the cathode side of the paper and makes it wet. The length traversed by ethanol on the cathode side of the strip in a given time is measured for different concentrations. It is found that higher concentrations led to faster cross over. The fuel utilization is generally low for these cells, and hence only a small fraction of the fuel participates in the reactions. Since the cell delivers the maximum power density (MPD) of 2.74 mW cm^{-2} and current density of 6.28 mA cm^{-2} at 4 M ethanol, in this study it is chosen as the best fuel concentration to work with. The rest of the experiments reported in this work are performed at 4 M ethanol + 4 M H_2SO_4, (anolyte) and 0.3 M $K_2Cr_2O_7$ + 4 M H_2SO_4 (catholyte). In addition to this, it is also observed that the stability of the cell does not significantly depend on the length of the arm. In fact for these type of cells, the flow rates and the fuel utilization are very low. If the products accumulate around the electrode, then it will start affecting the OCV and stability of the cell. This will happen if the length of the arm is small. A comparison of the cell performance for different arm lengths is shown in Fig. S2 of the supplementary information. It can be clearly observed that the case with short arm length leads to much lower performance as compared to other cases. Hence the length of the longer arm is kept at 8 cm.

3.3. Role of MoO_3 NRs catalyst

In order to improve the cell performance, MoO_3 NRs are used as the catalyst at the anode for accelerating the ethanol oxidation reaction. Cell performances at various loadings of MoO_3 NRs at the anode are shown in Fig. 5.

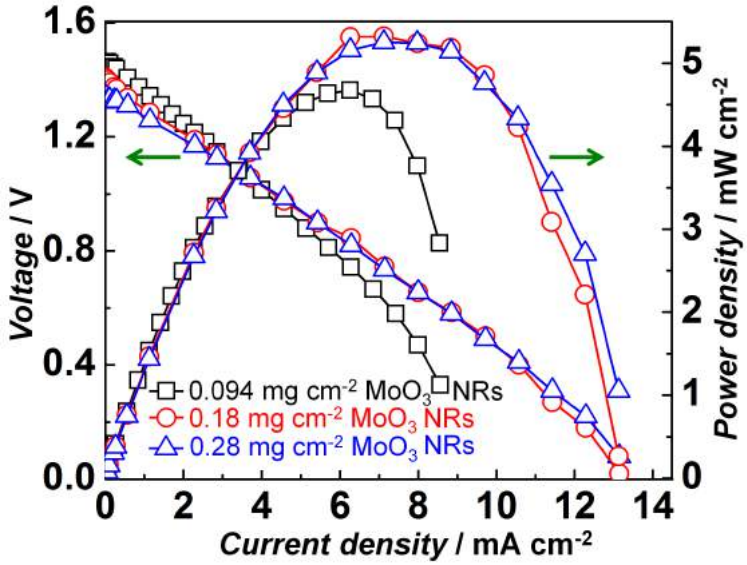

Figure 5: Cell performance at various catalyst (MoO_3 NRs) loadings. Anode is SS/carbon cloth/MoO_3 NRs and cathode is SS/carbon cloth. Anolyte is 4 M ethanol + 4 M H_2SO_4 and catholyte is 0.3 M $K_2Cr_2O_7$ + 4 M H_2SO_4.

Catalyst free carbon cloth is used as the cathode. MoO_3 NRs are prepared by hydrothermal routes and then dispersed in toluene and drop-cast at the anode. The catalyst loading is optimized on the basis of the maximum power density delivered by the cell. The maximum power density increases from 4.67 mW cm^{-2} to 5.32 mW cm^{-2} as the MoO_3 NRs loading is increased from 0.09 to 0.18 mg cm^{-2}. This is an expected result because of the increase in active sites with higher catalyst loading. As ethanol oxidation rate is generally slow, availability of large amounts of three phase boundary (TPB) area can lead to higher rates for the electrochemical reactions. Higher catalyst loading usually leads to increase in the TPB and hence increase in the exchange current density. No significant improvement in the cell performance is observed by increasing the oxide loading further, probably due to the agglomeration of particles. Therefore, the loading of MoO_3 NRs is maintained at 0.18 mg cm^{-2} for the rest of the experiments.

The electrocatalytic effect of MoO_3 NRs for ethanol oxidation and dichromate reduction is studied by loading them individually on the anode, cathode and then on both the electrodes. In all cases, the loading is maintained at 0.18 mg cm^{-2}. Figure 6 shows that the cell performance with

MoO_3 NRs is better than cell performance obtained using blank carbon cloth as electrode.

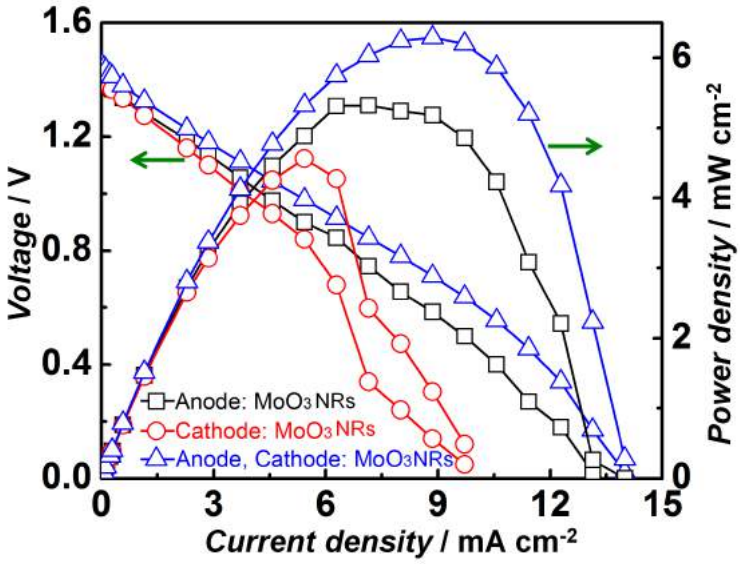

Figure 6: Cell performance for different electrode combinations with 0.18 mg cm^{-2} MoO_3 NRs loading. Anolyte is 4 M ethanol + 4 M H_2SO_4. Catholyte is 0.3 M $K_2Cr_2O_7$ + 4 M H_2SO_4.

With MoO_3 NRs as the anode electrocatalyst, the cell delivers a maximum power density of 5.32 mW cm^{-2}, which is higher than the maximum power density obtained using blank carbon cloth by almost 200%. With MoO_3 NRs as the cathode electrocatalyst, the maximum power density improves by 166% compared to blank carbon cloth. The best cell performance with 230% improvement (6.28 mW cm^{-2}) over blank carbon cloth electrodes is achieved when MoO_3 NRs are present at both the electrodes. This confirms that MoO_3 NRs catalyze both ethanol oxidation and dichromate reduction and therefore are suitable as low cost ecofriendly catalysts for these cells.

3.4. Comparison of MoO_3 NRs versus Ag nanoparticles (Ag NPs) as catalyst

In order to benchmark the performance of MoO_3 NRs, it is compared against Ag nanoparticles, which is reported to have good electro-oxidation kinetics for ethanol. For instance, Ag NPs supported on TiO_2 nanotubes [18] and bimetallic alloys containing Ag, such as, Pd/Ag [19] have

shown high electro-catalytic activity towards ethanol electro-oxidation. Since MoO_3 NRs have been employed as stand-alone catalysts in this work, Ag NPs were synthesized and incorporated as catalysts by drop casting onto the carbon cloth for comparing the performance of MoO_3 NRs against Ag NPs. The synthesis and UV/vis analysis of Ag NPs are discussed in the supplementary information (Fig. S3).

The presence of Ag NPs on both the electrodes leads to very low OCV of 0.66 V, possibly because of the following reasons: (i) The reaction between Ag and $K_2Cr_2O_7$ present at the cathode in an acidic medium, resulting in the formation of by-products, such as K_2SO_4 and $Ag_2Cr_2O_7$. (ii) The dilution effect caused by the formation of by-products. Therefore, this study was not considered for comparing the cell performance with MoO_3 NRs. The cell gave a better performance when Ag NPs were only present at the anode, and it was compared with the performance obtained with MoO_3 NRs. The corresponding I-V plots are presented in Fig. S4 of the supplementary information. It can be seen that the maximum power density obtained using Ag NPs (5.06 mW cm^{-2}) results in an increment of 87% compared to the base case (no catalyst), where the maximum power density attained was nearly 2.7 mW cm^{-2}. However, the performance of Ag NPs as an electro-catalyst for the redox couple considered in this study is inferior compared to the performance of MoO_3 NRs, which lead to a peak power density of 6.28 mW/cm^2. Thus, MoO_3 NRs prove to be better catalysts for both ethanol oxidation and dichromate reduction, unlike Ag NPs, which can favor the oxidation of only ethanol. Additionally, the use of Ag NPs or any noble metal catalyts, is not justified where the main aim is to develop cheap and cost-effective energy devices.

3.5. Cell performance at an elevated temperature

The cell performance is measured at 50 °C by placing the fully assembled cell with MoO_3 NRs present at anode and cathode, on a hot plate where the temperature was maintained at 50 °C. The corresponding I-V plot for the cell performance is shown in Fig. S5 of the supplementary information. The OCV obtained at this temperature is 0.8 V, which is much lower than the OCV achieved at room temperature (1.44 V). Ethanol is volatile and tends to evaporate at 50 °C,

resulting in a low fuel concentration in the anolyte. The change in Gibb' s free energy at higher temperature may also lead to drop in OCV. Hence, lower OCV and power density of 0.4 mWcm^{-2} are obtained at this temperature. Therefore, the cell performance is likely to deteriorate beyond 50 °C. Nevertheless, even at elevated temperatures, the cell is capable of delivering power and the performance is comparable to that of a paper based microbial fuel cell [20].

3.6. Electrochemical impedance spectra studies

The electrochemical impedance spectra (EIS) for the paper cells are recorded at various anolyte concentrations and constant catholyte concentration (0.3 M $K_2Cr_2O_7$ + 4 M H_2SO_4) with 0.18 mg cm^{-2} of MoO_3 NRs loading on both the electrodes. The Nyquist plots at open circuit conditions (OCV) are shown in Fig. 7(a) and at part load conditions (V_{cell} = 0.8 V) are shown in Fig. 7(b). The measurements are done in the frequency range of 1 MHz - 0.1 Hz, with a sinusoidal voltage perturbation of amplitude 10 mV.

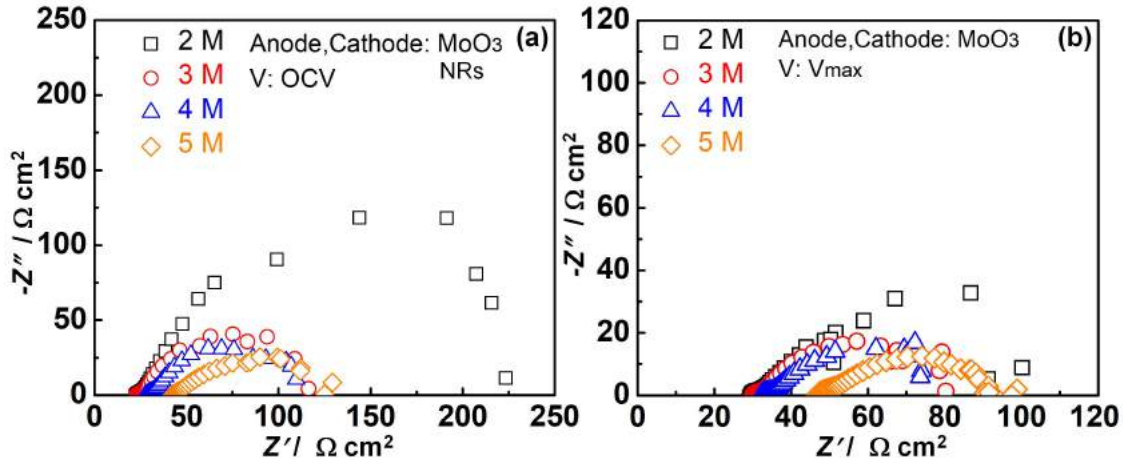

Figure 7: Electrochemical impedance spectra (EIS) of ethanol-dichromate fuel cell at (a) OCV and (b) V_{cell} = V_{max} = 0.8 V over a frequency scan range between 1 MHz-0.1 Hz at different fuel concentrations in 4 M H_2SO_4. MoO_3 NRs loading is 0.18 mg cm$-^2$ at both the electrodes.

In both Fig. 7(a) and Fig. 7(b), only a single arc is observed in the EIS data, indicating that the relaxation frequencies of the anodic and the cathodic processes are of the same time scale. Slight

scattering of data is observed in the low frequency regions. Ideally the EIS has to be recorded at steady state conditions, however, due to the eventual cross-over of the anolyte and catholyte over time, the cell voltage (or current in the case of potentiostatic mode) drops and does not allow the recording of EIS data under steady state conditions. The slight variations in the high frequency intercept is because of the variations in the fuel concentration, which leads to a change in the ohmic resistance of the cell. As explained earlier, the rate of cross-over of ethanol through the gel increases with increasing concentration, which alters the ionic conductivity of the Na-PSS/PVA/H^+ gel. The charge transfer resistance (R_{ct}) decreases with increase in concentration. For the measurements done at OCV, R_{ct} is maximum at 2 M ethanol with 200.6 Ω-cm^2 due to sluggish kinetics at low concentrations and at 4 M ethanol the cell produces a minimum R_{ct} of 81.7 Ω-cm^2, due to relatively faster kinetics. The trend is similar at V_{cell}=0.8 V; 2 M ethanol results in R_{ct} of 70.63 Ω-cm^2 and 4 M ethanol leads to 41.37 Ω-cm^2. Ideally during fuel cell operation R_{ct} decreases with increasing cell polarization [1, 21]. Thus the decrease in R_{ct} observed here at V_{cell}=0.8 V is in accordance with typical fuel cell operation. The lower R_{ct} at 4 M ethanol leads to better performance of the cell compared to other concentrations as observed in the dc-polarization measurements (Fig. 4). The internal resistance of the cell is the total resistance (R_{total}=R_{ohm}+R_{ct}), observed in the EIS spectra recorded at different fuel concentrations. Since the R_{ohm} and R_{ct} vary with the fuel concentration, R_{total} varies from 80.3 Ω cm^2 to 100.4 Ω cm^2, as the ethanol concentration is varied from 2 M to 5 M.

The Bode plots corresponding to Fig. 7(a) and Fig. 7(b) are shown in Fig. S6 and S7 (supplementary information), respectively. The scattering of the data due to unsteady cell operation at low frequency is clearly evident in the Bode plots. The characteristic frequencies are marked in all the plots. In all cases, the phase angle corresponding to the characteristic frequency is below 45 degree, indicating that process can not be presented using a pure RC circuit. For pure RC circuits, the phase angle reaches to 45 degree at the characteristic frequency. A small inductance component is observed at the high frequency limit, probably due to the wiring and contact, which

becomes effective at frequencies around 100 kHz to 1 MHz. Although the inductance part is not shown in the Nyquist plot, the Bode representations, clearly show the presence of inductance.

The capability of the paper based cell to power low power consuming devices for a short time is demonstrated by lighting a red LED. Two paper cells described in this work are stacked and then packed into a box-like acrylic scaffold designed and developed in our lab. Figure 8 shows the packaged cell in operation and illuminating an LED without any external bias. For the purpose of stacking, the cells are supported in acrylic sheets with appropriately positioned holes for feeding the anolyte and the catholyte to the cells. A schematic representation of the cell assembly is shown in Fig. 8(b).

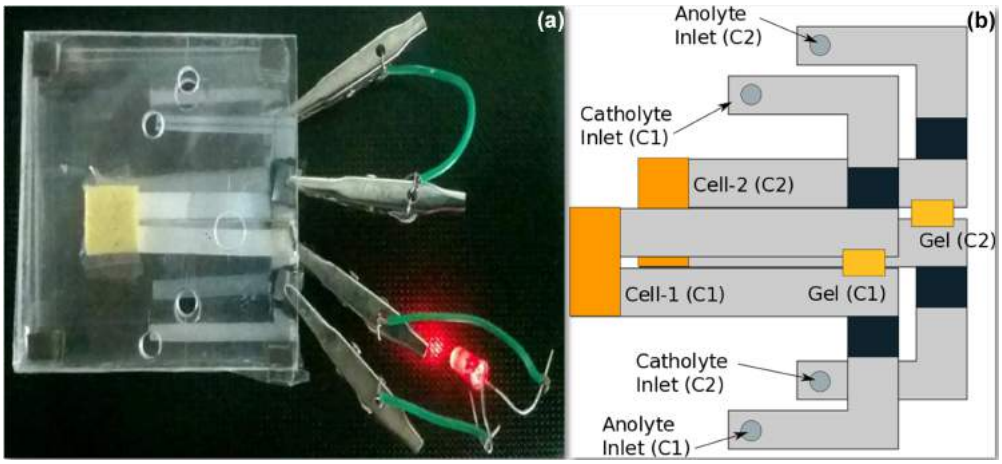

Figure 8: (a) Two paper cells stacked in series (dual cell stack), illuminating a LED, with an output cell voltage of 2.12 V (measured with multimeter). Anolyte is 4 M ethanol + 4 M H_2SO_4. Catholyte is 0.3 M $K_2Cr_2O_7$ + 4 M H_2SO_4. Catalyst loading is 0.18 mg cm^{-2} Mo_3 NRs. (b) A schematic of the dual cell stack assembly.

The anolyte and catholyte are discharged using a dropper and crocodile clips are used to make the connections. The LED serves as a load for the cell. The output voltage of the cell as measured using a multimeter is 2.12 V. The overall current flowing through the cells connected in series is 4.1 mA. Since the cells are connected in series, the same magnitude of current flows through both the cells. The cell assembly could power the LED for more than 40 minutes without the replenishing the anode and cathode with anolyte and catholyte.

This demonstration shows that this stack can be used for powering micro-analytical devices like a pregnancy test kit, glucometer, dengue detection kits and other visual monitoring based micro-nano devices. It can even replace the traditional non-rechargeable batteries which are typically used in such devices. Compared to batteries, this cell is made up of non-toxic components and thus, can be disposed easily without posing any threat to the environment. Unlike the non-rechargeable batteries used in these devices, the fuel cell here can be easily revived by simply dispensing ethanol and dichromate solutions through the holes provided. These solutions can be provided in air-tight vials.

In order to establish the durability of the cell over a long period of 8 hours, the current density obtained from the cell is plotted against time with an interval of 2 hours and is shown in Fig. S8 of the supplementary information. Here, the anolyte (4 M ethanol) and catholyte (0.3 M $K_2Cr_2O_7$) were dispensed only once during each interval, and the measurements were done by chronoamperometry method under potentiostatic conditions, i.e., at a constant voltage of 0.2 V. It can be seen that the initial cell current density of 12 mA cm^{-2} is steady for 10 minutes, and the same trend is observed after an interval of 2 hours with a slight decrease in the current density, which further drops to 10.5 mA cm^{-2} at later times. The measurements recorded after 4 and 6 hours show trivial instability in the cell performance. Nevertheless, it is found that the cell could still deliver a current density of more than 9 mA cm^{-2} even after 6 hours.

4. Conclusions

Paper-based ethanol-dichromate fuel-oxidant microfluidic cells with ethanol as the fuel, dichromate as the oxidant, MoO_3 NRs as the anode-cathode catalyst and a Na-PSS/PVA/H^+ gel, were assembled and characterized by various electrochemical measurements. Hydrothermally synthesized MoO_3 NRs were characterized by electron microscopy confirming the formation of nanorods with crystalline orthorhombic lattice structure. The cell delivered an OCV of 1.42 V and 2.74 mW cm^{-2} peak power density without any catalyst loading using an anolyte containing 4 M ethanol

and catholyte containing 0.3 M $K_2Cr_2O_7$. At the same conditions, with 0.18 mg cm^{-2} of MoO_3 NRs catalyst loading, the cell delivered an OCV of 1.42 V and a peak power density of 5.32 mW cm^{-2}. The cell voltage was more stable for a cell with MoO_3 NRs catalyst loaded at anode, as compared to cell without any catalyst. In order to further improve the cell performance, 0.18 mg cm^{-2} of catalyst was deposited on both the electrodes, and the power density increased to 6.32 mW cm^{-2}. Cyclic voltametry studies performed confirms the occurrence of multiple rate limiting charge transfer reactions at different voltages. Furthermore, the electroactive area increases with catalyst loading on the electrodes. EIS studies reveal that the polarization resistance of the cell increases with decrease in fuel concentration and the relaxation frequencies are of the same order for different cell processes. Finally the capability of the cell to power low power consuming devices is demonstrated by illuminating an LED using a stack of two cells connected in series and packaged into acrylic sheets based assembly. This clearly shows the potential of this cell as an alternative to batteries for powering micro-analytical devices.

Supplementary material

The synthesis and characterization of Ag NPs, dc-polarization curves for different channel lengths, bode plots corresponding to the EIS spectra, durability of the paper cell and images of the single cell and two cell stack, after 1 hour and 24 hours of operation, respectively.

References

[1] S. Lal, V. M. Janardhanan, M. Deepa, A. Sagar, K. C. Sahu, Low cost environmentally benign porous paper based fuel cells for micro-nano systems, J. Electrochem. Soc. 162 (14) (2015) F1402–F1407.

[2] R. Veerubhotla, A. Bandopadhyay, D. Das, S. Chakraborty, Instant power generation from an air-breathing paper and pencil based bacterial bio-fuel cell, Lab Chip 15 (12) (2015) 2580–2583.

[3] M. M. Gong, D. Sinton, Turning the page: advancing paper-based microfluidics for broad diagnostic application, Chem. Rev 117 (12) (2017) 8447–8480.

[4] S.-S. Chen, C.-W. Hu, I.-F. Yu, Y.-C. Liao, J.-T. Yang, Origami paper-based fluidic batteries for portable electrophoretic devices, Lab Chip 14 (12) (2014) 2124–2130.

[5] S. M. Mousavi Ehteshami, M. Asadnia, S. N. Tan, S. H. Chan, Paper-based membraneless hydrogen peroxide fuel cell prepared by micro-fabrication, J. Power Sources 301 (2016) 392–395.

[6] R. K. Arun, S. Halder, N. Chanda, S. Chakraborty, A paper based self-pumping and self-breathing fuel cell using pencil stroked graphite electrodes, Lab Chip 14 (10) (2014) 1661.

[7] J. Esquivel, F. Del Campo, J. De La Fuente, S. Rojas, N. Sabaté, Paper-based microfluidic fuel cells, 17th International Conference on Miniaturized Systems for Chemistry and Life Sciences, MicroTAS 2013 2 (October) (2013) 1251–1253.

[8] R. Verma, S. Lal, M. Deepa, V. M. Janardhanan, K. C. Sahu, Sodium percarbonate based, mixed-media fuel cells supported on paper with gold/nickel oxide catalysts, ChemElectroChem 4 (2) (2017) 310–319.

[9] A. J. Armenta-González, R. Carrera-Cerritos, A. Moreno-Zuria, L. Álvarez-Contreras, J. Ledesma-García, F. M. Cuevas-Muñiz, L. G. Arriaga, An improved ethanol microfluidic fuel cell based on a PdAg/MWCNT catalyst synthesized by the reverse micelles method, Fuel 167 (2016) 240–247.

[10] C. López-Rico, J. Galindo-de-la Rosa, E. Ortiz-Ortega, L. Álvarez-Contreras, J. Ledesma-Garcia, M. Guerra-Balcázar, L. Arriaga, N. Arjona, High performance of ethanol co-laminar flow fuel cells based on acrylic, paper and pd-nio as anodic catalyst, Electrochim. Acta 207 (2016) 164–176.

[11] A. Modjtahedi, A. Amirfazli, S. Farhad, Low catalyst loaded ethanol gas fuel cell sensor, Sens. Actuators, B 234 (2016) 70–79.

[12] S. Carrión-Satorre, M. Montiel, R. Escudero-Cid, J. Fierro, E. Fatás, P. Ocón, Performance of carbon-supported palladium and palladium ruthenium catalysts for alkaline membrane direct ethanol fuel cells, Int. J. Hydrog. Energy 41 (21) (2016) 8954–8962.

[13] L. Wang, P. Gao, D. Bao, Y. Wang, Y. Chen, C. Chang, G. Li, P. Yang, Synthesis of crystalline/amorphous core/shell MoO3 composites through a controlled dehydration route and their enhanced ethanol sensing properties, Cryst. Growth Des. 14 (2) (2014) 569–575.

[14] A. De, J. Datta, I. Haldar, M. Biswas, Catalytic Intervention of MoO_3 toward Ethanol Oxidation on PtPd Nanoparticles Decorated MoO_3-Polypyrrole Composite Support, ACS Appl. Mater. Interfaces 8 (42) (2016) 28574–28584.

[15] J. S. Chen, Y. L. Cheah, S. Madhavi, X. W. Lou, Fast Synthesis of a -MoO_3 Nanorods with controlled aspect ratios and their enhanced lithium storage capabilities, J. Phys. Chem. C (2010) 8675–8678.

[16] Y. Wang, Y. Zhu, Z. Xing, Y. Qian, Hydrothermal synthesis of α-MoO_3 and the influence of later heat treatment on its electrochemical properties, Int. J. Electrochem. Sci. 8 (7) (2013) 9851–9857.

[17] L. T. Døssland, Electro-oxidation of ethanol at Pt electrodes with the use of a dynamic electrochemical

impedance spectroscopy (DEIS) technique, Master Thesis, Department of Materials Science and Engineering, Norwegian University of Science and Technology (2012) 85.

[18] Y. Liang, Z. Cui, S. Zhu, Y. Liu, X. Yang, Silver nanoparticles supported on tio 2 nanotubes as active catalysts for ethanol oxidation, J. Catal. 278 (2) (2011) 276–287.

[19] N. Abbasi, P. Shahbazi, A. Kiani, Electrocatalytic oxidation of ethanol at Pd/Ag nanodendrites prepared via low support electrodeposition and galvanic replacement, J. Mater. Chem. A 1 (34) (2013) 9966–9972.

[20] A. Fraiwan, S. Mukherjee, S. Sundermier, H.-S. Lee, S. Choi, A paper-based microbial fuel cell: Instant battery for disposable diagnostic devices, Biosens. Bioelectron. 49 (2013) 410–414.

[21] B. Prasad, V. M. Janardhanan, Modeling sulfur poisoning of Ni-based anodes in solid oxide fuel cells, J. Electrochem. Soc. 161 (3) (2014) 208–213.